Joint International Topical Meeting on Mathematics & Computation and Supercomputing in Nuclear Applications (M&C + SNA 2007)
Monterey, California, April 15-19, 2007, on CD-ROM, American Nuclear Society, LaGrange Park, IL (2007)

SHOCK WAVE SOLUTIONS FOR RADIATION HYDRODYNAMICS

Robert B. Lowrie
Los Alamos National Laboratory
Computer and Computational Sciences Division
Computational Physics and Methods Group (CCS-2), MS D413
Los Alamos, NM 87545
lowrie@lanl.gov

Jarrod D. Edwards
Department of Nuclear Engineering
Texas A & M University
College Station, TX 77843
jdedwards@tamu.edu

ABSTRACT

This study describes a semi-analytic solution of planar radiative shock waves in which the radiation model is grey nonequilibrium diffusion. The solution may be used to verify radiation-hydrodynamics codes. Comparisons are made with the equilibrium diffusion solutions of Lowrie and Rauenzahn [1]. Although the physics of radiative shocks are fairly well known, previous solutions have been approximate and therefore unsuitable for code verification. Previous work has also assumed that the material temperature reaches its maximum at the post-shock state of the embedded hydrodynamic shock (Zel'dovich spike). We show that in certain cases, the temperature may actually continue to increase after the hydrodynamic shock and reaches its maximum at a specific value of the local Mach number. This is the first semi-analytic solution we know of for high-energy density, nonequilibrium radiation hydrodynamics.

Key Words: Radiation Hydrodynamics, Shock Waves, Verification

1. INTRODUCTION

This study describes a semi-analytic solution for planar radiative shocks in which the radiation model is grey nonequilibrium diffusion. It is an extension of the work of Lowrie and Rauenzahn [1] who considered solutions in the equilibrium diffusion (1-T) limit. The solutions described here may be used to verify radiation hydrodynamics codes that use the nonequilibrium diffusion radiation model. The solution procedure requires finding numerically the root of a polynomial and integrating a pair of coupled nonlinear ordinary differential equations. Because a numerical procedure is still required, we refer to our solutions as "semi-analytic." Compared with a finite-difference approach, errors are more easily controlled with our semi-analytic approach and it offers additional insight into the shock structure.

Verification is critical to ensuring that a code is accurately solving the governing equations. For multiphysics codes such as coupled radiation hydrodynamics, verification is typically extremely difficult, as analytic (or even semi-analytic) solutions are often non-existent. The semi-analytic solution we outline in this study is the first we know of for high-energy density, nonequilibrium radiation-hydrodynamics.

The physics of radiative shocks is described in detail by Zel'dovich and Raizer [2] and Mihalas and Mihalas [3]. Aside from the 1-T work of Lowrie and Rauenzahn [1], solutions in past work are typically approximate

and thus inappropriate for code verification. By "approximate," we mean either terms are dropped or the solution is from a finite-difference calculation; see Refs. [4–7] for some examples.

The focus of this study is an extension the work of Ref. [1] to a grey nonequilibrium diffusion model. The paper is organized as follows: In §2, we state the full governing equations that are solved. Section 2 states the shock problem and reviews the structure of radiative shocks. The reduced set of equations is derived in §4 and the solution procedure is outlined in §5. Sample solutions are given in §6 and we explain why the temperature may increase after the embedded hydrodynamic shock in §7.

The solutions given here are for constant cross-sections. In addition, the resulting equations are very stiff, particularly at large Mach number. We have been unable to obtain reliable solutions above a Mach number of about 30. Future work will address these issues.

2. GOVERNING EQUATIONS

The radiation hydrodynamics model used in this study is the single-material, nonrelativistic Euler equations, coupled with grey nonequilibrium diffusion (see [8]):

$$\partial_t \rho + \partial_x(\rho v) = 0, \tag{1a}$$

$$\partial_t(\rho v) + \partial_x\left(\rho v^2 + p + \frac{1}{3}\mathcal{P}_0\phi\right) = 0, \tag{1b}$$

$$\partial_t(\rho E) + \partial_x\left[v(\rho E + p)\right] = \mathcal{P}_0\sigma_a(\phi - T^4) - \frac{1}{3}\mathcal{P}_0 v\partial_x\phi, \tag{1c}$$

$$\partial_t\phi + \frac{4}{3}\partial_x(v\phi) - \partial_x(\kappa\partial_x\phi) = -\sigma_a(\phi - T^4) + \frac{1}{3}v\partial_x\phi, \tag{1d}$$

where ρ is the material density, v the material velocity, p the material pressure, T the material temperature, ϕ the radiation energy density, and E the material specific total energy, defined as

$$E = e + \frac{1}{2}v^2, \tag{2}$$

where e is the specific internal energy. The absorption and total cross-sections are assumed to have the functional dependence $\sigma_a(\rho, T)$ and $\sigma_t(\rho, T)$. We also assume a perfect gas equation-of-state (EOS), which for our nondimensionalization, gives

$$p = \frac{\rho T}{\gamma}, \qquad e = \frac{T}{\gamma(\gamma - 1)}, \tag{3}$$

where γ is the ratio of specific heats.

In this study, dimensional quantities are denoted with a tilde; for example, $\tilde{p}$. The nondimensional variables are defined in terms of their dimensional counterparts as

$$x = \frac{\tilde{x}}{\tilde{L}}, \quad t = \frac{\tilde{t}\tilde{a}_0}{\tilde{L}}, \quad \rho = \frac{\tilde{\rho}}{\tilde{\rho}_0}, \quad v = \frac{\tilde{v}}{\tilde{a}_0}, \quad e = \frac{\tilde{e}}{\tilde{a}_0^2}, \tag{4}$$

$$p = \frac{\tilde{p}}{\tilde{\rho}_0\tilde{a}_0^2}, \quad T = \frac{\tilde{T}}{\tilde{T}_0}, \quad \phi = \frac{\tilde{\phi}}{\tilde{\alpha}_R\tilde{T}_0^4}, \quad \sigma_a = \frac{\tilde{\sigma}_a\tilde{L}\tilde{c}}{\tilde{a}_0}, \quad \kappa = \frac{\tilde{c}}{3\tilde{\sigma}_t\tilde{a}_0\tilde{L}},$$

where the subscript-"$_0$" indicates a constant reference state. Here $\tilde{a}$ refers to the material sound speed, $\tilde{L}$ is a reference length, $\tilde{\alpha}_R$ is the radiation constant, and $\tilde{c}$ the speed of light. The nondimensional constant $\mathcal{P}_0$ is given by

$$\mathcal{P}_0 = \frac{\tilde{\alpha}_R \tilde{T}_0^4}{\tilde{\rho}_0 \tilde{a}_0^2}. \tag{5}$$

The sum of Eqs. (1c) and $\mathcal{P}_0$ times (1d) gives the total energy relation

$$\partial_t(\rho E + \mathcal{P}_0\phi) + \partial_x\left[v\left(\rho E + p + \frac{4}{3}\mathcal{P}_0\phi\right)\right] = \mathcal{P}_0\partial_x(\kappa\partial_x\phi). \tag{6}$$

Strong solutions of the system (1) also satisfy

$$\rho\frac{De}{Dt} + p\partial_x v = \mathcal{P}_0\sigma_a(\phi - T^4). \tag{7}$$

For a given EOS, the character of the solution is determined by the shock Mach number ($\mathcal{M}_0 = \tilde{v}_0/\tilde{a}_0 = v_0$), the parameter $\mathcal{P}_0$, and the functions $\kappa(\rho, T)$ and $\sigma_a(\rho, T)$. The Mach number determines the strength of the shock. The constant $\mathcal{P}_0$ is a measure of the influence of radiation on the flow dynamics; $\mathcal{P}_0$ is proportional to the ratio of radiation pressure to material pressure and the radiation energy to material energy.

3. SHOCK PROBLEM STATEMENT

This section defines the shock problem. As with the equilibrium diffusion system considered in Ref. [1], the system (1) is Galilean invariant. Consequently, we can consider the steady-state reference frame, where the shock speed is zero. Once the shock profile is found, we can then easily transform to other reference frames. The flow is assumed to move in the $+x$ direction. The reference state (subscript-$_0$) will refer to the pre-shock conditions, attained as $x \to -\infty$, while the subscript-$_1$ refers to post-shock conditions, attained as $x \to \infty$. We assume that far from the shock the flow is in radiative equilibrium ($\phi = T^4$). The problem statement is then as follows:

- *Given:* The values γ, $\mathcal{M}_0$, $\mathcal{P}_0$, ρ_0, v_0, T_0, and the functions $\sigma_a(\rho, T)$ and $\kappa(\rho, T)$. Note that $\phi_0 = T_0^4$.
- *Calculate:* The functions $\rho(x)$, $v(x)$, $T(x)$, and $\phi(x)$.

3.1. Solution Phenomenology

In this section, we review the structure of radiative shocks. The physics of these shocks is explained very well in Refs. [2–6]; only the minimum information needed will be repeated here. As the material moves through the shock structure it passes through several regions, in the following order:

1. *Radiation Precursor:* The hot post-shock material radiates, heating the flow ahead of the shock from $T = T_0$ to $T = T_p > T_0$. The value of T_p determines the character of the shock:
   - Subcritical shock: $T_p < T_1$.
   - Supercritical shock: $T_p \equiv T_1$.

See Fig. 1.

2. For supercritical shocks and if $\rho_p \equiv \rho_1$, then all variables are continuous through the shock profile. If instead $\rho_p < \rho_1$ (true for all subcritical shocks), then the flow passes next through the following regions:

   (a) *Hydrodynamic Shock:* A hydrodynamic shock then further heats the material from $T = T_p$ to $T = T_s > T_1$. For the Euler equations, this heating is discontinuous. Note that even if the the state-$_p$ conditions are in radiative equilibrium the hydrodynamic shock discontinuity breaks equilibrium; the state-$_s$ is always a nonequilibrium state. The spike to $T = T_s$ is referred to as the *Zel'dovich spike* [3, 5, 6].

   (b) *Relaxation Region:* Through radiative cooling the material cools from $T = T_s$ to its final post-shock state, $T = T_1$. The width of the relaxation region is proportional to the post-shock optical depth.

Note that as a result of the diffusion term, ϕ is continuous through the shock.

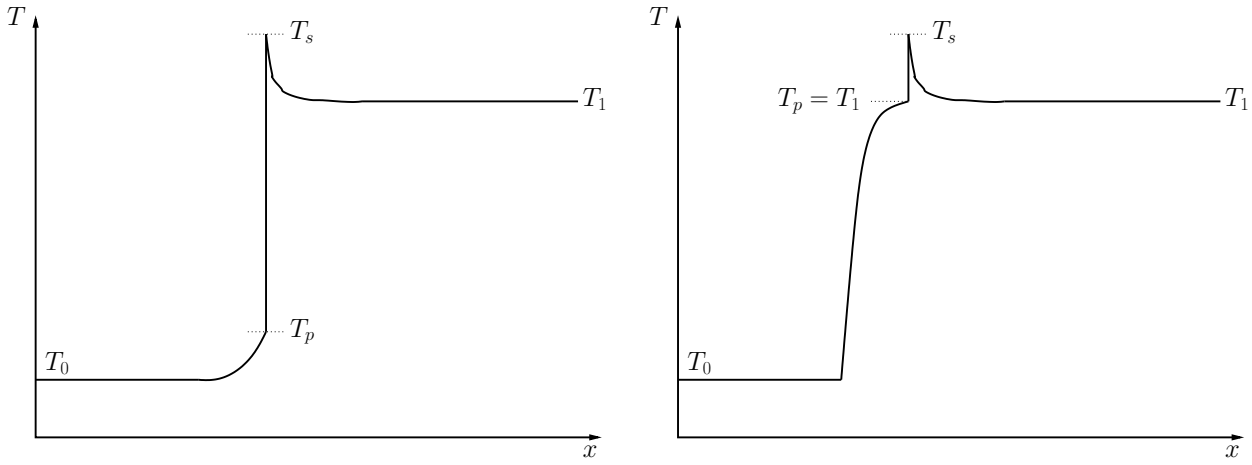

(a) Subcritical

(b) Supercritical

Figure 1. Subcritical and supercritical shock structures. In both cases, the temperature is discontinuous from T_p to T_s.

4. REDUCED EQUATIONS

In this section, we derive the reduced set of equations that satisfy the system (1) for the shock problem given in §3.

4.1. Overall Jump Conditions

To determine state-$_1$, we use the overall jump conditions as in Ref. [1]:

$$\begin{pmatrix} \rho v \\ \rho v^2 + p^* \\ (\rho E^* + p^*)v \end{pmatrix}_0 = \begin{pmatrix} \rho v \\ \rho v^2 + p^* \\ (\rho E^* + p^*)v \end{pmatrix}_1 , \tag{8}$$

where

$$p^* = p + \frac{1}{3}\mathcal{P}_0 T^4, \tag{9}$$

$$e^* = e + \frac{1}{\rho}\mathcal{P}_0 T^4, \tag{10}$$

$$E^* = e^* + \frac{1}{2}v^2. \tag{11}$$

These equations can be easily manipulated to a polynomial in T whose root must be found numerically; for the details, see Refs. [1, 9].

4.2. Jump Conditions at Zel'dovich Spike

At a steady discontinuity, the system (1) gives the following jump relations, separating state-$_p$ from state-$_s$ (see Fig. 1):

$$(\rho v)_p = (\rho v)_s, \tag{12a}$$

$$(\rho v^2 + p)_p = (\rho v^2 + p)_s, \tag{12b}$$

$$\left[v\left(\rho E + p\right)\right]_p = \left[v\left(\rho E + p\right)\right]_s , \tag{12c}$$

$$\left(-\kappa\partial_x\phi + \frac{4}{3}v\phi\right)_p = \left(-\kappa\partial_x\phi + \frac{4}{3}v\phi\right)_s , \tag{12d}$$

where we have used the fact that ϕ must be continuous. The first three relations are the standard hydrodynamic jump conditions. Note that Eq. (12d) states that the diffusive flux,

$$-\kappa\partial_x\phi,$$

is discontinuous at a shock. But the comoving-frame flux,

$$-\kappa\partial_x\phi + \frac{4}{3}v\phi,$$

is continuous.

4.3. Precursor and Relaxation Regions

In this section, we derive the ordinary differential equations that hold in the precursor and relaxation regions. In the steady-state frame ($\partial_t \equiv 0$), integrate equation (1a) to give

$$\rho v = v_0 \equiv \mathcal{M}_0. \tag{13}$$

The local Mach number, $\mathcal{M}$, is defined as

$$\mathcal{M} = \frac{v}{\sqrt{T}} = \frac{\mathcal{M}_0}{\rho\sqrt{T}}. \tag{14}$$

Integrate equation (1b) to obtain

$$3\gamma\frac{\mathcal{M}_0^2}{\rho} + 3\rho T + \gamma\mathcal{P}_0\phi = K_m, \tag{15}$$

where the constant K_m is given by

$$K_m = 3(\gamma\mathcal{M}_0^2 + 1) + \gamma\mathcal{P}_0. \tag{16}$$

Equation (15) is quadratic in ρ and the solution is

$$\rho(T,\phi) = \frac{K_m - \gamma\mathcal{P}_0\phi \pm \sqrt{(K_m - \gamma\mathcal{P}_0\phi)^2 - 36\gamma\mathcal{M}_0^2 T}}{6T}. \tag{17}$$

There are two roots, or branches. The "-"-branch always satisfies $\rho(T_0,\phi_0) = \rho_0 = 1$. Which branch satisfies $\rho(T_1,\phi_1) = \rho_1$ is problem dependent. Within the profile, the solution may switch branches through a shock wave or at a point where the discriminate is zero. More discussion of the branch points will be given below.

Next, integrate (6) and use (13) to yield

$$\phi' = \mathcal{M}_0\frac{6C_p(\rho^2 T - 1) + 3(\mathcal{M}_0^2 - 1) + 8\mathcal{P}_0(\rho\phi - 1)}{\mathcal{P}_0\kappa} \tag{18}$$

where $C_p = 1/(\gamma - 1)$ and $(\cdot)' = d(\cdot)/dx$. Steady solutions of Eq. (7) satisfy

$$\rho v e' + p v' = \mathcal{P}_0\sigma_a(\phi - T^4), \tag{19}$$

which reduces to

$$\frac{\mathcal{M}_0}{\gamma}\left(C_p T' - \frac{T}{\rho}\rho'\right) = \mathcal{P}_0\sigma_a(\phi - T^4). \tag{20}$$

Differentiate Eq. (15) to obtain

$$-3\gamma\frac{\mathcal{M}_0^2}{\rho^2}\rho' + 3(\rho T' + T\rho') + \gamma\mathcal{P}_0\phi' = 0, \tag{21}$$

or

$$\rho' = \rho^2\frac{3\rho T' + \gamma\mathcal{P}_0\phi'}{3(\gamma\mathcal{M}_0^2 - \rho^2 T)} \tag{22}$$

Substitute this expression into Eq. (20) to yield

$$T' = \mathcal{P}_0\frac{v\phi' + 3\sigma_a(\gamma\mathcal{M}^2 - 1)(\phi - T^4)}{3C_p\mathcal{M}_0(\mathcal{M}^2 - 1)}. \tag{23}$$

Equations (18) and (23) are two ordinary differential equations for ϕ and T, because knowing ϕ and T, we can find ρ from Eq. (17), p from Eq. (3), and v from Eq. (13).

4.4. Branch Points

From Eq. (17), there is a branch point in the solution whenever the discriminate vanishes, which occurs when

$$K_m - \gamma \mathcal{P}_0 \phi = \pm 6 \mathcal{M}_0 \sqrt{\gamma T}. \tag{24}$$

Substitute this expression back into Eq. (17) and recognize that only the "+"-root results in a nonnegative density, so that at the branch point

$$\rho = \mathcal{M}_0 \sqrt{\frac{\gamma}{T}}. \tag{25}$$

Using Eq. (13), this condition may be written in terms of the local Mach number as

$$\mathcal{M} = 1/\sqrt{\gamma} \equiv \mathcal{M}_b, \tag{26}$$

where we denote $\mathcal{M} = \mathcal{M}_b$ as the location of a branch point. Recall that Eq. (26) represents the Mach number of isothermal sound waves. In an isothermal flow, larger Mach numbers can result in isothermal shocks, such as those that may occur in radiative shocks predicted by the equilibrium diffusion model [1]. Because the pre- and post-shock Mach numbers of an isothermal shock must straddle $\mathcal{M}_b$, for the equilibrium diffusion model, branch points are always at the isothermal shock.

For nonequilibrium diffusion, the situation is more complicated. Isothermal shocks are not present, only full hydrodynamic shocks. If there is a branch point, it cannot be in the precursor, because $\mathcal{M}_0 > \mathcal{M}_p > 1$. The branch point is at the shock if $\mathcal{M}_s < \mathcal{M}_b$. A branch point exists in the relaxation region if $\mathcal{M}_s > \mathcal{M}_b > \mathcal{M}_1$. Whether $\mathcal{M}_1$ can surpass $\mathcal{M}_b$ will be the subject of future research, but if it does, it appears to occur at very large $\mathcal{M}_0$, which we have been unable to compute reliably at this time.

4.5. Mach Number as the Independent Variable

In this section, we change the independent variable from x to $\mathcal{M}$. Using $\mathcal{M}$ as the independent variable will allow us to integrate through branch points and singularities. It follows from Eq. (14) that

$$\mathcal{M}' = -\mathcal{M}\left(\frac{\rho'}{\rho} + \frac{1}{2}\frac{T'}{T}\right), \tag{27}$$

so that

$$\frac{dx}{d\mathcal{M}} = \frac{-2\rho T}{\mathcal{M}(2T\rho' + \rho T')}. \tag{28}$$

Next, use Eq. (22) to obtain

$$\frac{dx}{d\mathcal{M}} = \frac{-6\rho T(\gamma\mathcal{M}^2 - 1)}{\mathcal{M}[2\gamma\mathcal{P}_0\phi' + 3\rho(\gamma\mathcal{M}^2 + 1)T']}. \tag{29}$$

In addition,

$$\frac{dT}{d\mathcal{M}} = \frac{dx}{d\mathcal{M}} T'. \tag{30}$$

Substitute Eq. (23) into eqs. (29,30) to yield

$$\frac{dx}{d\mathcal{M}} = \frac{3\mathcal{M}_0(\mathcal{M}^2 - 1)\rho\beta}{\mathcal{P}_0}, \tag{31}$$

$$\frac{dT}{d\mathcal{M}} = (\gamma - 1)\beta\left[\mathcal{M}_0\phi' + (\gamma\mathcal{M}^2 - 1)r\right], \tag{32}$$

where

$$\beta = \frac{-2T}{\mathcal{M}\left[(\gamma+1)\mathcal{M}_0\phi' + (\gamma-1)(\gamma\mathcal{M}^2+1)r\right]} \tag{33}$$

and

$$r = 3\rho\sigma_a(\phi - T^4). \tag{34}$$

Note that Eq. (23) is singular at $\mathcal{M} = 1$ whereas Eqs. (31,32) are not. Although one may also substitute Eq. (18) into Eqs. (31,32) for ϕ', there is no apparent benefit in doing so.

Equations (31,32) represent an alternative system to Eqs. (18,23), but require that we can write ρ and ϕ in terms of T and $\mathcal{M}$. To this end, Eq. (14) gives that

$$\rho(T, \mathcal{M}) = \frac{\mathcal{M}_0}{\mathcal{M}\sqrt{T}}. \tag{35}$$

Also, Eq. (15) may be solved for ϕ:

$$\phi(T, \mathcal{M}) = \frac{1}{\gamma\mathcal{P}_0}\left[K_m - 3\gamma\frac{\mathcal{M}_0^2}{\rho(T,\mathcal{M})} - 3T\rho(T,\mathcal{M})\right], \tag{36}$$

To summarize this section, using $\mathcal{M}$ as the independent variable results in the following:

- Equations (35,36) do not require the choice of a branch cut, unlike Eq. (17).
- Equations (31,32) are nonsingular at $\mathcal{M} = 1$, unlike Eq. (23). Unfortunately, Eqs. (31,32) are singular whenever the solution is constant, which occurs as $x \to \pm\infty$. Consequently, x must be the independent variable near the far-field states.
- Given integration endpoints $\mathcal{M} = \mathcal{M}_A$ and $\mathcal{M} = \mathcal{M}_B$, we must assume that $\mathcal{M}$ is monotone between $\mathcal{M}_A$ and $\mathcal{M}_B$. However, the validity of this assumption is easily checked because x is updated via Eq. (31). If the resulting x is non-monotone, then our assumption is violated. We have yet to encounter non-monotone behavior.

5. SOLUTION PROCEDURE

We define the radiation temperature as

$$\theta = \phi^{1/4}. \tag{37}$$

The solution procedure is then as follows:

1. Find $(\rho, v, T)_1$ by solving the system (8) as in Ref. [1]. Set $\theta_1 = T_1$.
2. Find the foot of the precursor:
   (a) Set $\theta_\varepsilon = 1.001$, or some small value that represents a value in the precursor such that $1 < \theta_\varepsilon < \theta_1$

(b) Use a shooting method to find the corresponding T_ε by integrating Eqs. (18,23) in the $-x$ direction, to match state-$_0$ as $x \to -\infty$.

3. Find the remainder of the precursor by integrating Eqs. (31,32) from state-$_\varepsilon$ until $\mathcal{M} < 1$ or $\theta > \theta_1$. Generally, a hydrodynamic shock will lie somewhere on this precursor.

4. Search for the shock location ($x_p = x_s$) on the precursor by applying the hydrodynamic jump conditions, integrating to $x \to \infty$, and then checking whether the state-$_1$ conditions are met. If $\mathcal{M}_s > \mathcal{M}_b > \mathcal{M}_1$, then a branch point exists somewhere downstream of the shock. If there is branch point, break the x-integration into two stages:

   (a) Integrate Eqs. (31,32) from $\mathcal{M} = \mathcal{M}_s$ to $\mathcal{M} \equiv \mathcal{M}_{\text{stop}} = (\mathcal{M}_1 + \mathcal{M}_b)/2$.

   (b) Integrate Eqs. (18,23) from $x = x_{\text{stop}}$ to $x \to \infty$.

   If there is no branch, integrate Eqs. (18,23) from $x = x_s$ to $x \to \infty$.

6. SAMPLE SOLUTIONS

In this study, we present results for constant cross-sections. Results for variable cross-sections will be left for future work; see Ref. [1] for such results for equilibrium diffusion. Thus far in our calculations we have been able to obtain results up to about $\mathcal{M}_0 \approx 30$. For higher $\mathcal{M}_0$, the equations become very stiff and we are currently unable to obtain solutions with our numerical procedure.

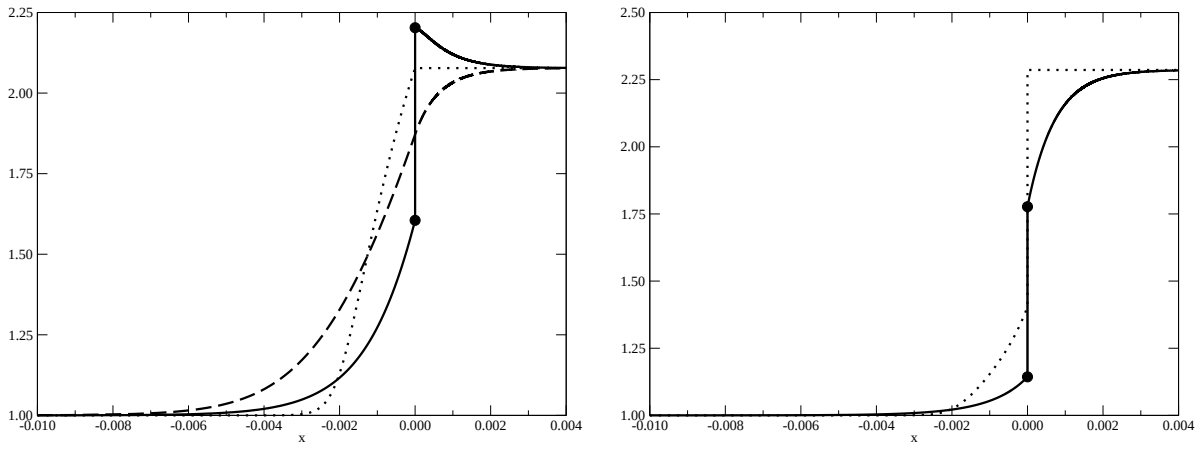

(a) Temperature: Solid T, dashed θ, dotted T("1-T")

(b) Density: Solid ρ, dotted ρ("1-T")

Figure 2. Results for $\mathcal{M}_0 = 2$, $\mathcal{P}_0 = 10^{-4}$, $\sigma_a = 10^6$, $\kappa = 1$, $\gamma = 5/3$. The symbols denote the endpoints of the embedded hydrodynamic shock. The "1-T" results (equilibrium diffusion) are generated using the procedure from Ref. [1].

Results for $\mathcal{M}_0 = 2$ are shown in Fig. 2 compared with equilibrium-diffusion results using the procedure from Ref. [1]. Note how the entire profile is out of equilibrium $(T \neq \theta)$. This shock is clearly subcritical which as discussed in Ref. [1], equilibrium-diffusion theory cannot predict. At $\mathcal{M}_0 = 3$, the shock remains barely subcritical as shown in Fig. 3. The Zel'dovich spike narrows and the precusor extent is larger.

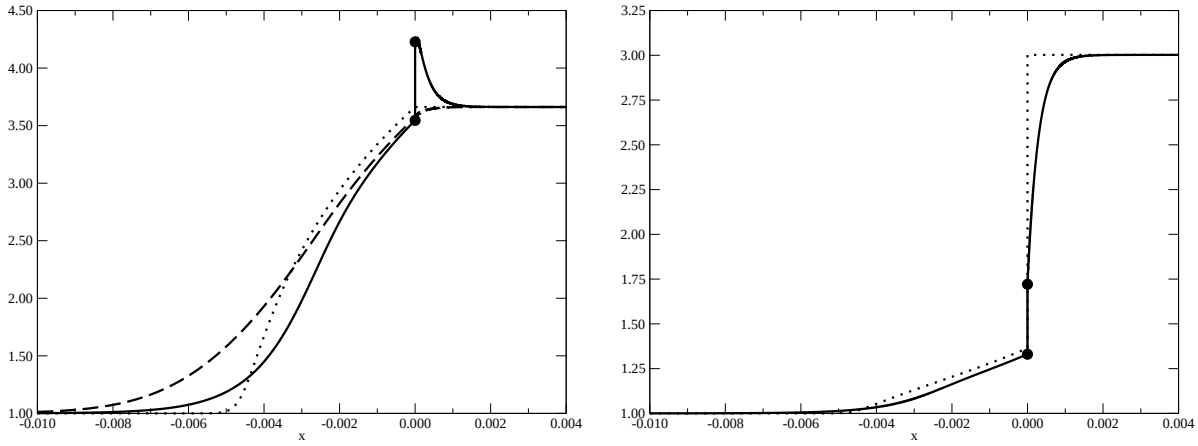

(a) Temperature: Solid T, dashed θ, dotted T("1-T")

(b) Density: Solid ρ, dotted ρ("1-T")

Figure 3. Same conditions as Fig. 2, but with $\mathcal{M}_0 = 3$.

Figure 4 shows the results for $\mathcal{M}_0 = 5$. The shock is now supercritical with a much larger precursor and an extremely narrow Zel'dovich spike. Much of the precursor is in equilibrium, except near the foot. The details of the spike region are shown in Fig. 5. As discussed in Ref. [1], the equilibrium diffusion theory completely ignores the spike. Most interesting is that the material temperature continues to rise after the hydrodynamic shock. We do not believe this temperature rise has been recognized in previous work and we offer an explanation for this phenomenon in the next section.

7. MAXIMUM TEMPERATURE

In this section, we offer an explanation as to why for the $\mathcal{M}_0 = 5$ case, the material temperature continues to increase after the embedded hydrodynamic shock. For supercritical radiative shocks, a reasonable approximation is that $\phi' \approx 0$ in the Zel'dovich spike region, so that Eq. (23) gives

$$T'\big|_{x=x_s} \approx \frac{\gamma \mathcal{P}_0 \sigma_a}{C_p \mathcal{M}_0} \frac{(\mathcal{M}_s^2 - \mathcal{M}_b^2)(\theta_s^4 - T_s^4)}{(\mathcal{M}_s^2 - 1)}. \tag{38}$$

Using that fact that $\mathcal{M}_s < 1$ and $T_s > \theta_s$, whenever $\mathcal{M}_s > \mathcal{M}_b$, it is clear that $T'|_{x=x_s} > 0$. For the $\mathcal{M}_0 = 5$ case, these conditions are met, which explains the post-shock temperature increase shown in Fig. 5.

With the approximation $\phi' \approx 0$, Eq. (32) reduces to

$$\frac{dT}{d\mathcal{M}} \approx -\frac{2T}{\mathcal{M}} \frac{\mathcal{M}^2 - \mathcal{M}_b^2}{\mathcal{M}^2 + \mathcal{M}_b^2}. \tag{39}$$

Therefore, T reaches its maximum value when $\mathcal{M} \approx \mathcal{M}_b$. In other words, the maximum T occurs near the branch point as shown in Fig. 5.

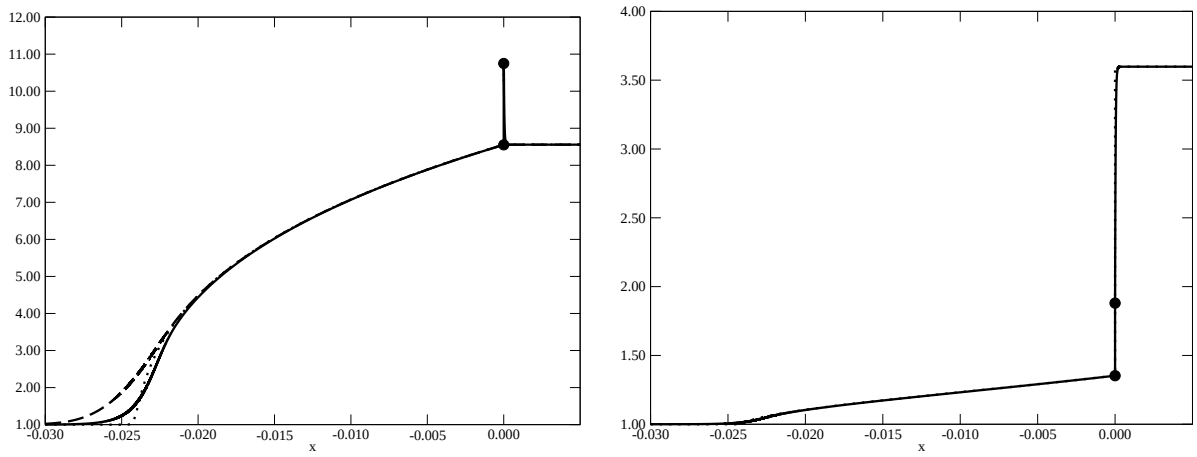

(a) Temperature: Solid T, dashed θ, dotted T("1-T")

(b) Density: Solid ρ, dotted ρ("1-T")

Figure 4. Same conditions as Fig. 2, but with $\mathcal{M}_0 = 5$.

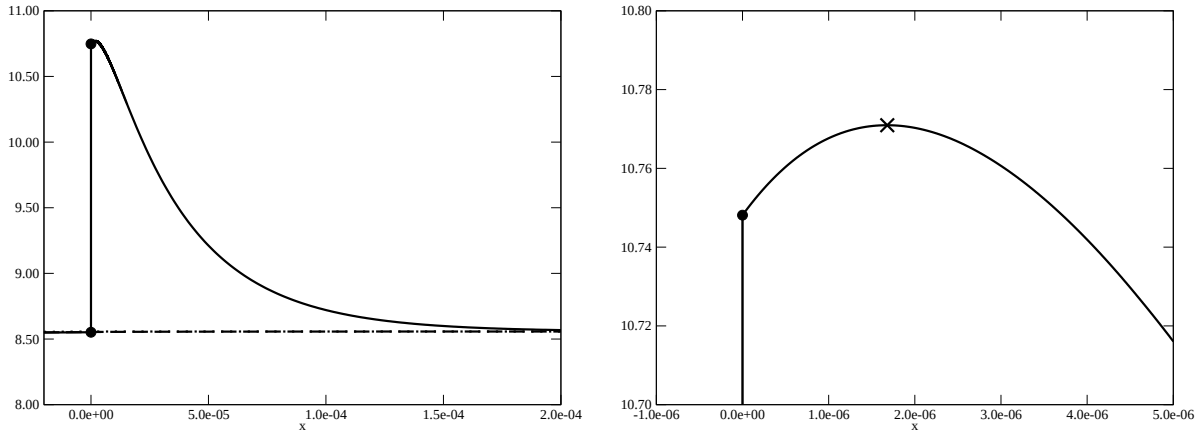

Figure 5. Detail of Zel'dovich spike region from Fig. 4a. The left plot shows the full relaxation region. The radiation temperature and "1-T" results coincide on this scale. The right plot shows the region of maximum T. The X symbol marks the branch point location.

For the $\mathcal{M} = 2, 3$ cases shown in Figs. 2,3, we find that $\mathcal{M}_s < \mathcal{M}_b$, so that T decreases monotonically in the relaxation region. In these cases, the branch point is at the hydrodynamic shock, because $\mathcal{M}_p > 1 > \mathcal{M}_b$.

We stress that the arguments in this section have assumed that $\phi' \approx 0$ in the relaxation region. However, these arguments should extend to more accurate radiation models as long as this assumption holds.

8. FUTURE WORK

We have only begun to explore the parameter space for radiative shocks with a nonequilibrium diffusion radiation model. In future work, we plan to fully investigate their structure and to resolve the issues with computing higher Mach number shocks. The character of the solutions with variable cross-sections will also be studied.

ACKNOWLEDGEMENTS

This work was performed under the auspices of the U.S. Department of Energy under contract DE-AC52-06NA25396 and is also available as Los Alamos Technical Report LA-UR-07-1077.

REFERENCES

[1] R. B. LOWRIE and R. M. RAUENZAHN, "Radiative shock solutions in the equilibrium-diffusion limit," Tech. Rep. LA-UR-06-8283, Los Alamos National Laboratory, 2006. Submitted to the journal *Shock Waves*.

[2] Y. B. ZEL'DOVICH and Y. P. RAIZER, *Physics of Shock Waves and High-Temperature Hydrodynamic Phenomena*. Dover, 2002.

[3] D. MIHALAS and B. W. MIHALAS, *Foundations of Radiation Hydrodynamics*. Oxford University Press, New York, 1984.

[4] M. A. HEASLET and B. S. BALDWIN, "Predictions of structure of radiation-resisted shock waves," *Physics of Fluids*, vol. 6, no. 6, pp. 781 – 791, 1963.

[5] M. W. SINCELL, M. GEHMEYR, and D. MIHALAS, "The quasi-stationary structure of radiating shock waves. I. The one-temperature fluid.," *Shock Waves*, vol. 9, no. 6, pp. 391 – 402, 1999.

[6] M. W. SINCELL, M. GEHMEYR, and D. MIHALAS, "The quasi-stationary structure of radiating shock waves. II. The two-temperature fluid.," *Shock Waves*, vol. 9, no. 6, pp. 403 – 11, 1999.

[7] C. P. WANG, "Effect of thermal radiation on the propagation of plane shock waves.," *Physics of Fluids*, vol. 13, no. 7, pp. 1717 – 24, 1970.

[8] J. E. MOREL, "The grey diffusion approximation in the Eulerian and comoving frames to O(v/c)," Tech. Rep. CCS-2:04-08(U), Los Alamos National Laboratory, 2004.

[9] S. BOUQUET, R. TEYSSIER, and J. P. CHIEZE, "Analytical study and structure of a stationary radiative shock.," *Astrophysical Journal Supplement Series*, vol. 127, no. 2, pp. 245 – 52, 2000.